research papers

Inhibition of *Leishmania major* pteridine reductase by 2,4,6-triaminoquinazoline: structure of the NADPH ternary complex

**Karen McLuskey,[a] Federica
Gibellini,[a,b] Paulo Carvalho,[c]
Mitchell A. Avery[c] and
William N. Hunter[a]***

[a]Division of Biological Chemistry and Molecular
Microbiology, School of Life Sciences,
University of Dundee, Dundee DD1 5EH,
Scotland, [b]Dipartimento di Scienze
Farmaceutiche, Universita di Modena e Reggio
Emilia, Via Campi 183, 41100 Modena, Italy,
and [c]Department of Medicinal Chemistry,
School of Pharmacy, National Center of Natural
Product Research, University of Mississippi,
MS 38677, USA

Correspondence e-mail:
w.n.hunter@dundee.ac.uk

The structure of *Leishmania major* pteridine reductase (PTR1) in complex with NADPH and the inhibitor 2,4,6-triaminoquinazoline (TAQ) has been solved in a new crystal form by molecular replacement and refined to 2.6 Å resolution. The inhibitor mimics a fragment, the pterin head group, of the archetypal antifolate drug methotrexate (MTX) and exploits similar chemical features to bind in the PTR1 active site. Despite being a much smaller molecule, TAQ displays a similar inhibition constant to that of MTX. PTR1 is a target for the development of improved therapies for infections caused by trypanosomatid parasites and this analysis provides information to assist the structure-based development of novel enzyme inhibitors.

1. Introduction

Trypanosomatid protozoans, *e.g. Trypanosoma* and *Leishmania* species, are the causal agents of a range of serious human diseases in the tropical and subtropical areas of the world (Webster, 1990). The current treatments of these infections involve drugs such as sodium stibogluconate and nifurtimox that induce serious side-effects and this, together with the increase in drug-resistant parasites, has created an urgent requirement for new more effective treatments (Fairlamb, 2003). Improved knowledge of trypanosomatid biology and biochemistry promotes an understanding of how existing drugs function and serves to identify novel enzyme targets for chemotherapeutic attack (Beverley *et al.*, 2002; Beverley, 2003). The ideal targets are enzymes proven to be essential for the survival of the parasite and that are either absent from the human host or, if present, display markedly differing substrate specificities.

One area that has provided useful targets and therapies for cancer and microbial infection is folate metabolism and in particular the enzymes thymidylate synthase (TS) and dihydrofolate reductase (DHFR) (Bermingham & Derrick, 2002; Walsh, 2003; Then, 2004). All cells require TS and DHFR activities. TS catalyses the conversion of dUMP to dTMP using the cofactor N^5,N^{10}-methylene tetrahydrofolate (THF) as both the C-donor and reductant, whilst DHFR maintains the THF pool by the NADPH-dependent reduction of dihydrofolate (DHF). Inhibition of either enzyme limits the supply of dTMP required for DNA synthesis, thus curtailing replication and leading to cell death. Both TS and DHFR have been extensively characterized and targeted for chemotherapy, especially DHFR, which is the classical target for antibacterial and antineoplastic therapy (Blakely, 1995).

Since folates and pterins are essential for the growth of the parasitic trypanosomatids, the enzymes associated with this aspect of their metabolism are of interest as drug targets and

the use of antifolates should in principle provide an ideal treatment. However, DHFR inhibitors are largely ineffective for the control of trypanosomatid infection partly owing to the presence of a short-chain dehydrogenase/reductase (SDR) family member, pteridine reductase (PTR1; Nare *et al.*, 1997). Genetic experiments indicate that PTR1 activity is essential for parasite growth *in vitro* (Cunningham & Beverley, 2001; Cunningham *et al.*, 2001). This NADPH-dependent enzyme exhibits a broad pteridine-reductase activity and is capable of reducing both unconjugated (biopterin) and conjugated (folate) pterins from either the oxidized or dihydro state. Since the latter activity duplicates that of DHFR, PTR1 can function as a metabolic bypass to alleviate antifolate inhibition

of DHFR. However, an inhibitor of PTR1 has the potential to act in concert with known potent DHFR inhibitors to provide a new approach to the treatment of trypanosomatid infection.

High-resolution crystal structures of *L. major* PTR1–ligand complexes have provided details of protein–pterin inter-actions and in conjunction with biochemical data clearly defined a sequential two-step reduction mechanism (Luba *et al.*, 1998; Gourley *et al.*, 2001). The first catalytic step resem-bles other SDR-family members and exploits three residues in particular to (i) position the nicotinamide of the cofactor NADPH for hydride transfer (Lys198), (ii) acquire a proton from solvent (Asp181) and (iii) pass this over onto the substrate (Tyr194). The second reduction step, which occurs on the opposite side of the pterin, is similar to that postulated for DHFR. Nicotinamide again provides a hydride ion and an activated water molecule supplies the proton. The structure of the ternary complex of PTR1, NADPH and the antifolate methotrexate (4-amino-N^{10}-methyl-pteroylglutamic acid; MTX; Fig. 1*a*) described a mode of inhibition and, in conjunction with the dihydrobiopterin (DHB) complex, the structural basis for the enzyme's broad substrate specificity.

We are now engaged in a search for potent inhibitors of PTR1, seeking to exploit the structural information available. Analysis of the PTR1–NADPH–MTX ternary complex suggested that the *p*-aminobenzoic (*p*ABA) moiety might not contribute that much to enzyme inhibition and we sought to characterize a smaller entity bound within the active site. We now report the details of a complex formed with 2,4,6-tri-aminoquinazoline (TAQ; Fig. 1*b*).

2. Material and methods

2.1. Chemical synthesis of TAQ

The synthesis of TAQ was based on literature methods (Davoll & Johnson, 1970; Rudisill & Stille, 1989). In brief, anthranilonitrile (50 mmol; 5.9 g) and cyanoguanidine (50 mmol; 4.2 g) were dissolved in 25 ml 2 *N* hydrochloric acid and stirred under reflux. After 2 h, 375 ml hot water, 65 ml 2 *N* sodium hydroxide and 500 mg charcoal were added. The mixture was then filtered and cooled to room temperature, resulting in a precipitate of 2,4-diaminoquinazoline. This was filtered, washed with ethanol and ether and air-dried to produce 5.22 g of product (66% yield).

A sample of 2,4-diaminoquinazoline (20 mmol; 3.2 g) was dissolved in 90 ml hot water and treated with 6 ml concen-trated nitric acid. The mixture was cooled on ice, producing a white precipitate that was filtered off, washed with ice water and then added to a cooled mixture of 18.6 ml concentrated nitric acid and 18.6 ml concentrated sulfuric acid. After 15 min, the mixture was allowed to reach room temperature and then stirred for 1 h. This solution was added to 200 g crushed ice and the mixture basified with ammonium hydroxide. The orange precipitate of 2,4-diamino-6-nitro-quinazoline was collected, washed with cold water, ethanol and ether and air-dried. The yield for this step was 87.8% (3.6 g).
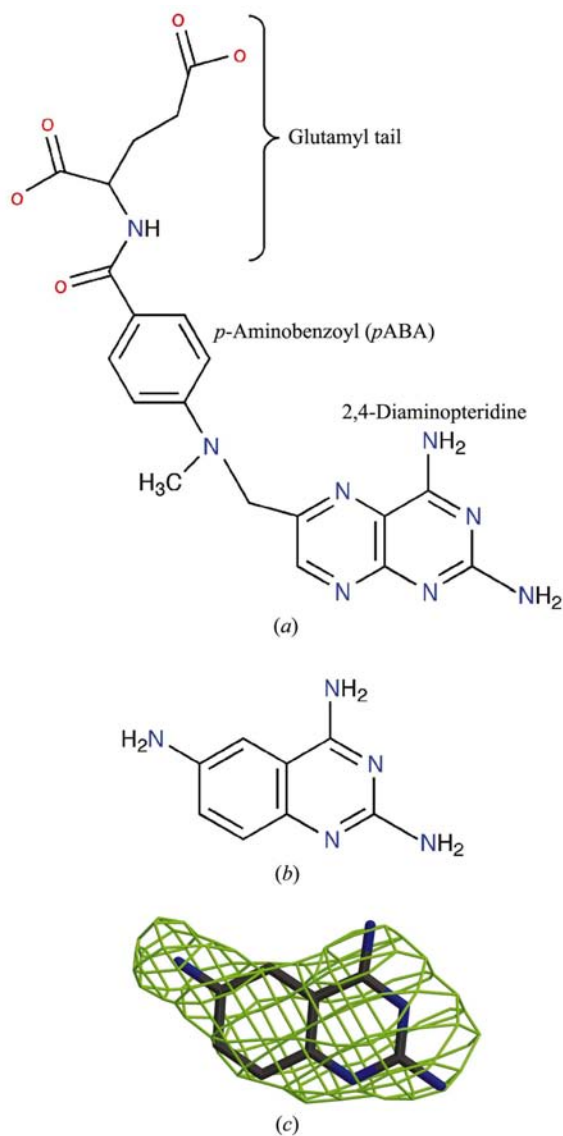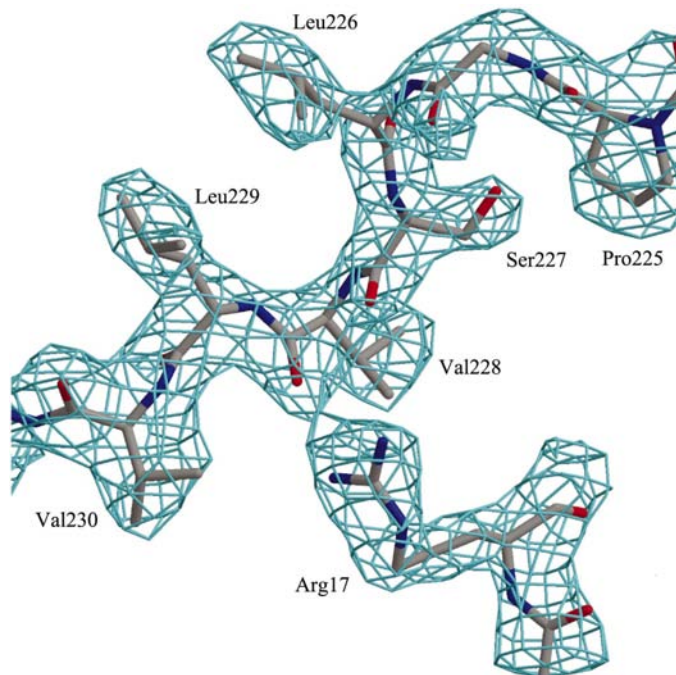

Figure 1
The chemical structures of (*a*) methotrexate (MTX) and (*b*) 2,4,6-triaminoquinazoline (TAQ). (*c*) The difference density omit map (light green chicken wire) for TAQ in active site *A*, calculated with ($|F_o - F_c|$), α_c coefficients and contoured at the 3σ level. F_o represents the observed structure factors, F_c the calculated structure factors and α_c the calculated phases. The atoms shown in this image (black represents C-atom positions, blue N atoms) did not contribute to F_c or α_c.

2,4-Diamino-6-nitroquinazoline (14.6 mmol; 3 g) was dissolved in 55 ml ethanol and treated with 60 ml glacial acetic acid. Iron powder (4 g) was added and the mixture refluxed for 2 h before being neutralized with a saturated solution of potassium carbonate and extracted with dichloromethane. The organic layers were combined, dried with magnesium sulfate, filtered through silica gel and the solvent removed to leave 1.7 g TAQ (65% yield).

2.2. PTR1 inhibition and crystallographic analysis

The expression and purification of *L. major* PTR1 followed published methods (Gourley *et al.*, 1999) and the inhibition of the enzyme by TAQ, with respect to folate, was determined following an established protocol (Hardy *et al.*, 1997). This provided an IC_{50} value of 2.0 µM.

A ternary complex of PTR1 with TAQ and NADPH was prepared by adding 2 ml 20 mM sodium acetate pH 5.3 containing 1 mM NADPH, 1 mM TAQ, 20 mM DTT and 1% DMSO to 0.2 ml PTR1 at a concentration of 10 mg ml^{-1}. This mixture was incubated at room temperature for 1 h and the volume then reduced to 0.2 ml with centrifugal concentrators. This sample was used to obtain crystals using the hanging-drop method for vapour diffusion. A drop containing 2 µl complex solution plus 2 µl of a reservoir solution consisting of 11–14% PEG 5000, 100 mM sodium acetate buffer pH 5.5 and 40–140 mM calcium acetate was set up against reservoir solution at 293 K. The crystals grew as clumps of thin fragile rods, from

Table 1
Data-collection, refinement and model geometry statistics.

Resolution (Å)	2.6
Wavelength (Å)	0.939
No. measurements	255759
No. unique reflections	83228
Redundancy	3.9
Completeness (%)	91.0 (85.2†)
$I/\sigma(I)$	6.9 (2.8†)
R_{merge} (%)	14.6 (10.1‡) (40.6†)
Wilson B factor (Å^2)	33
Protein residues (total)	2147
In subunits A–H	279, 276, 266, 258, 269, 272, 265, 262
Protein atoms (total)	17473
Solvent atoms	1122
R_{work} (%) (No. reflections)	26.7 (79067)
R_{free} (%) (No. reflections)	33.7 (4162)
Average isotropic thermal parameters (Å^2)	
Subunits A–H	19, 19, 20, 20, 20, 20, 22, 22
NADPH	15
TAQ	15 (28§)
Solvents	15
R.m.s.d. bonds	0.012
R.m.s.d. bond angles (°)	1.355
Ramachandran analysis	
Favoured regions (%)	87.2
Additionally allowed regions (%)	12.6

† Values refer to the highest resolution bin (2.7–2.6 Å). ‡ Value refers to the low resolution bin (30.0–5.6 Å). § Refers to the TAQ molecule bound on the surface of subunit A.

which fragments were cleaved for analysis, cryopreserved by transferring through a solution consisting of 70% reservoir solution and 30% glycerol and flash-cooled to 100 K in a stream of nitrogen gas.

The samples invariably displayed diffraction patterns commensurate with multiple crystals and/or suffered mechanical damage and many were tried before acceptable diffraction data were obtained. Data were collected using station ID14 EH4 at the European Synchrotron Research Facility (ESRF, Grenoble, France) and processed using *DENZO/SCALEPACK* (Otwinowski & Minor, 1997). The space group is $P2_1$, with unit-cell parameters a = 95.85, b = 102.95, c = 146.71 Å, β = 108.3°. PTR1 is a homotetramer with a subunit of 288 amino acids and a molecular weight of 25.7 kDa; the asymmetric unit contains two such tetramers (subunits are labelled A–H). The search model was a PTR1 tetramer (PDB code 1e92) and each oligomer was independently positioned by molecular replacement (*AMoRe*; Navaza, 1994) and refined using *REFMAC* (Murshudov *et al.*, 1997) combined with graphics inspection and model/map fitting with *O* (Jones *et al.*, 1991). The *CCP*4 suite of programs was used for the analysis (Collaborative Computational Project, Number 4, 1994). A conservative approach to the identification of water molecules was adopted in which only sites in difference density maps equal to or greater than 2.5σ and which had one or more contacts to potential hydrogen-bonding partners within the distance criteria 2.5–3.6 Å were included for refinement. Sites for which isotropic thermal parameters exceeded 45 Å^2 or for which there was only poor electron density after refinement were subsequently deleted. A total of 1122 solvent positions are included in the final

Figure 2
An example of the electron density (cyan chicken wire) for residues on one side of the active site. The map was calculated with ($|2F_o − F_c|$), α_c coefficients and contoured at the 1.5σ level. The residues are depicted in stick mode and coloured according to atom type; C, grey; N, blue; O, red. The real-space fit residual (RSF; Jones *et al.*, 1991) was calculated for the whole structure and the average value per residue is 90%. Each residue is this figure has an RSF of approximately 90% and can therefore be taken as representative of the fit of the model to electron density.

model, which is equivalent to one water molecule for every two amino-acid residues. A bulk-solvent scattering correction was also applied. Non-crystallographic symmetry restraints were imposed on certain less flexible elements of secondary structure throughout the refinement process.

We note that most of the model, including all of the active-site regions, is well defined by the electron density (for example, see Figs. 1c and 2). However, a concern that arose during refinement was the value of R_{free} and the 7% discrepancy with R_{work}. This was perhaps not surprising given the quality of the diffraction data; for example, the R_{merge} to 5.6 Å resolution is about 10% (Table 1). In addition, the electron-density and difference-density maps in the areas of several surface loops displayed strong features that could not be satisfactorily modelled. We assume that a combination of static and conformational disorder is present and that the R_{work} and R_{free} values are likely to contain a significant contribution from the density that we have been unable to model.

3. Results and discussion

3.1. Structure description

The PTR1 subunit is a single α/β-domain comprising a seven-stranded parallel β-sheet with three α-helices on either side. The arrangement of these elements of secondary structure is similar to that of the classical Rossmann fold. The functional tetramer, with 222-point group symmetry, carries two active sites on each side of the assembly separated by only 25 Å. In this crystal structure the asymmetric unit consists of eight subunits, or two tetramers. Since we incorporated NCS restraints on elements of secondary structure and because comparisons indicate a high level of conservation (data not shown), it is only necessary to describe one active site; we arbitrarily choose that associated with subunit A to detail.

The active site is an elongated L-shaped cleft (Fig. 3) of about 22 × 15 Å, mainly created by C-terminal sections of several of the β-strands, two sections of α-helix and an extended loop region (Gourley *et al.*, 2001). The C-terminus of a partner subunit blocks one end of the active site and places Arg287′ (′ identifies a contribution from another subunit) directed towards the catalytic centre. The cofactor binds in the active site in an extended conformation, with the nicotinamide creating the floor of the catalytic centre and Phe113 forming an overhang under which the pterin-binding pocket is formed. Nearby are three important residues. Tyr194 is the active-site base, which acts in concert with Asp181 to acquire and pass on one reducing equivalent. Lys198 helps to position the nicotinamide by virtue of hydrogen-bonding interactions with the cofactor ribose and this basic side chain may also reduce the pK_a of Tyr194 and in so doing assist catalysis.

A network of hydrogen bonds organizes the active site and serves to position the enzyme cofactor. Some of these inter-actions are depicted in Fig. 4. Notably, Asn147 forms inter-actions with Lys198 and Ser111, which position the latter two residues to bind the nicotinamide ribose. The amide group of
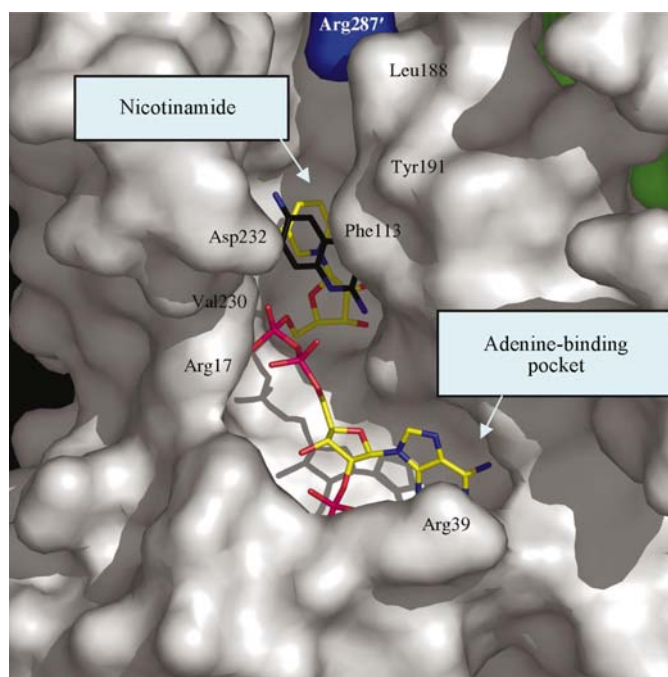
Figure 3
The active-site cleft of PTR1. The surface of subunit A is shown in grey, the surface of subunit B in green and Arg287′ from subunit D in blue. The cofactor and inhibitor are represented in stick mode and coloured according to atom type: N, blue; O, red; P, pink; C, yellow for NADPH and black for TAQ. Selected residues that line the active-site cleft are labelled. Figs. 3, 4 and 5 were prepared with *PyMOL* (DeLano, 2002).
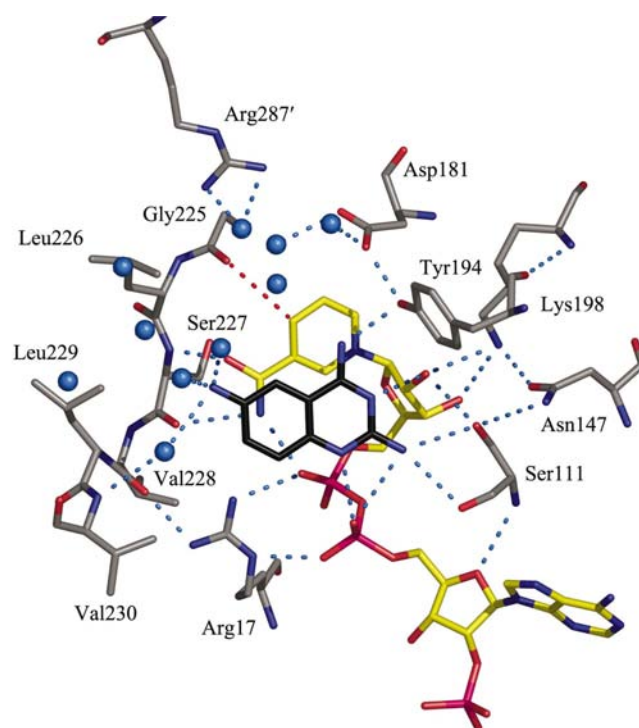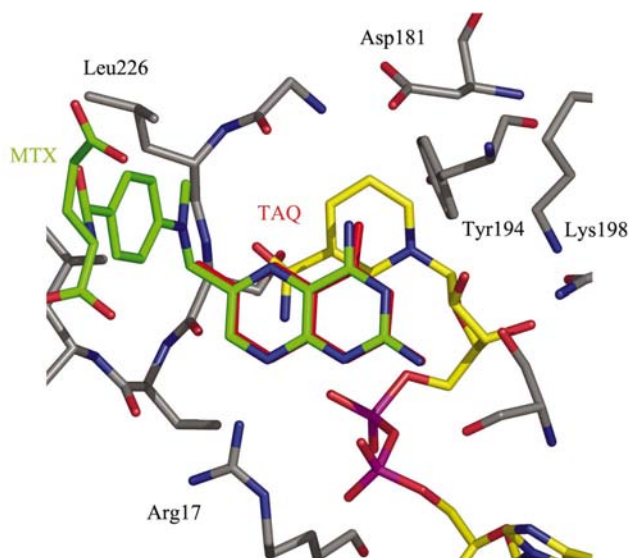

Figure 4
Hydrogen-bonding interactions at the site of inhibition. A similar colour scheme to Figs. 2 and 3 is adopted; in addition, water molecules are depicted as marine-coloured spheres. Marine dashed lines represent possible hydrogen-bonding associations and a red dashed line represents the C—H···O interaction between C5 (*) and the carbonyl of Gly225.

Ser111 is also able to donate a hydrogen bond to O4′ of the adenine ribose. Arg17 interacts with the main-chain carbonyl of Val228 and plays a critical role in binding the cofactor pyrophosphate. The main-chain amide and carbonyl groups of Ser227 form hydrogen bonds with the carboxyamide group of the nicotinamide, which in turn forms an interaction with the nearby cofactor phosphate. Finally, the carbonyl group of Gly225 participates in a C—H···O hydrogen bond with the nicotinamide C5.

TAQ occupies the pterin-binding pocket, sandwiched between the nicotinamide and Phe113, with all five functional groups participating in hydrogen-bonding interactions (Fig. 4). The 6-amino group interacts with three water molecules, which are highly conserved in all eight subunits of the asymmetric unit. The 4-amino group donates a hydrogen bond to Tyr194 OH. The 2-amino group interacts with the side-chain OG and the main-chain carbonyl group of Ser111 and also with a cofactor phosphate group. The latter two contacts may represent a bifurcated hydrogen bond. The inhibitor N3 atom accepts a hydrogen bond donated by the 2′-hydroxyl group on the nicotinamide ribose. The inhibitor N1 is 2.8 Å from a phosphate of the cofactor. This strongly suggests the formation of a hydrogen bond between these two groups and therefore protonation is likely to have occurred. This is noteworthy since it has been proposed that this cofactor phosphate group is a temporary acceptor for a proton during PTR1 catalysis (Gourley et al., 2001).

On the other side of the TAQ is a cavity between the inhibitor and Arg287′ which opens up to the surface of the protein. A number of ordered water molecules making numerous hydrogen-bonding interactions with Arg287′, Asp181 and each other occupy this section of the active-site cleft.

A well ordered molecule of TAQ is also observed bound on the surface of PTR1 near the loop linking $\beta 3$ and $\alpha 3$ of subunit A and is held in place by van der Waals interactions with the loop and solvent-mediated hydrogen bonds to the protein. Nearby, but not interacting with this ligand, is a symmetry-related loop (not shown).

3.2. Comparison with MTX

Previous crystallographic analysis shows that MTX interacts with PTR1 mainly using the pterin moiety (Fig. 1), participating in similar hydrogen-bonding interactions as TAQ does with both the cofactor and Tyr194. The MTX pABA moiety and glutamyl tail are relatively flexible and only loosely associated with PTR1 (Gourley et al., 2001). MTX is a more potent inhibitor of DHFR (IC$_{50}$ = 0.005 μM; Hardy et al., 1997) than PTR1 (IC$_{50}$ = 1.1 μM) because the pABA group makes more extensive interactions, including two direct salt-bridge associations with residues in the DHFR active site (e.g. Knighton et al., 1994). An interesting observation from early studies on DHFR is that the pteridine moiety of MTX binds in that active site in a different orientation to that adopted by the substrate (Charlton et al., 1985). Likewise, PTR1 binds its substrates biopterin and DHB with the pteridine rotated about the N2–N5 axis 180° relative to MTX (Gourley et al., 2001).

TAQ and MTX inhibit recombinant L. major PTR1 with IC$_{50}$ values of 2.0 and 1.1 μM (Hardy et al., 1997), respectively, and an overlay (Fig. 5) indicates that the pterin-like head groups bind to the active site of the enzyme in very similar fashion. It is noteworthy that despite being a much smaller entity, TAQ displays a comparable level of inhibition as is observed for MTX.

4. Conclusions

We have determined the structure of a new crystal form of L. major PTR1 in complex with the inhibitor TAQ at 2.6 Å resolution. This quinazoline derivative mimics the pterin head group of the well studied antifolate MTX, but despite being a much smaller molecule displays a comparable IC$_{50}$ value. The presence of a solvent-filled cavity, occupied by conserved water molecules and lined by hydrophilic residues (Asp181 and Arg287′), suggests a suitable region to target by covalent modification to the quinazoline framework. This might now allow the development of improved PTR1 inhibitors with potential to be novel antileishmanial drugs.

Figure 5
Superposition of TAQ on MTX based on an overlay of the PTR1 subunits in the respective structures. The view and colour scheme are similar to Fig. 4, although MTX C atoms are green and TAQ is entirely red. Hydrogen bonds and water molecules have been omitted for the purpose of clarity.

References

Bermingham, A. & Derrick, J. P. (2002). *Bioessays*, **24**, 637–648.
Beverley, S. M. (2003). *Nature Rev. Genet.* **4**, 11–19.

Beverley, S. M., Akopyants, N. S., Goyard, S., Matlib, R. S., Gordon, J. L., Brownstein, B. H., Stormo, G. D., Bukanova, E. N., Hott, C. T., Li, F., MacMillan, S., Muo, J. N., Schwertman, L. A., Smeds, M. R. & Wang, Y. (2002). *Philos. Trans. R. Soc. London Ser. B*, **357**, 47–53.

Blakely, R. L. (1995). *Adv. Enzymol. Relat. Areas Mol. Biol.* **70**, 23–102.

Charlton, P. A., Young, D. W., Birdsall, B. W., Feeney, J. & Roberts, G. C. K. (1985). *J. Chem. Soc. Perkin Trans.* **191**, 1349–1353.

Collaborative Computational Project, Number 4 (1994). *Acta Cryst.* **D50**, 760–763.

Cunningham, M. L. & Beverley, S. M. (2001). *Mol. Biochem. Parasitol.* **113**, 199–213.

Cunningham, M. L., Titus, R. G., Turco, S. J. & Beverley, S. M. (2001). *Science*, **292**, 285–287.

Davoll, J. & Johnson, A. M. (1970). *J. Chem. Soc. C*, **8**, 997–1002.

DeLano, W. L. (2002). *The PyMOL Molecular Graphics System.* DeLano Scientific, San Carlos, CA, USA.

Fairlamb, A. H. (2003). *Trends Parasitol.* **11**, 488–494.

Gourley, D. G., Luba, J., Hardy, L. W., Beverley, S. M. & Hunter, W. N. (1999). *Acta Cryst.* **D55**, 1608–1610.

Gourley, D. G., Schüttelkopf, A. W., Leonard, G. A., Luba, J., Hardy, L. W., Beverley, S. M. & Hunter, W. N. (2001). *Nature Struct. Biol.* **8**, 521–525.

Hardy, L. W., Matthews, W., Nare, B. & Beverley, S. M. (1997). *Exp. Parasitol.* **87**, 157–169.

Jones, T. A., Zou, J. Y., Cowan, S. W. & Kjeldgaard, M. (1991). *Acta Cryst.* **A47**, 110–119.

Knighton, D. R., Kan, C. C., Howland, E., Janson, C. A., Hostomska, Z., Welsh, K. M. & Matthews, D. A. (1994). *Nature Struct. Biol.* **1**, 186–194.

Luba, J., Nare, B., Liang, P. H., Anderson, K. S., Beverley, S. M. & Hardy, L. W. (1998). *Biochemistry*, **37**, 4093–4104.

Murshudov, G. N., Vagin, A. A. & Dodson, E. J. (1997). *Acta Cryst.* **D53**, 240–255.

Nare, B., Luba, J., Hardy, L. W. & Beverley, S. M. (1997). *Parasitology*, **114**, 101–110.

Navaza, J. (1994). *Acta Cryst.* **A50**, 157–163.

Otwinowski, Z. & Minor, W. (1997). *Methods Enzymol.* **276**, 307–326.

Rudisill, D. E. & Stille, J. K. (1989). *J. Org. Chem.* **54**, 5856–5866.

Then, R. L. (2004). *J. Chemother.* **16**, 3–12.

Walsh, C. (2003). *Antibiotics: Actions, Origins, Resistance.* Washington, DC, USA: ASM Press.

Webster, L. T. Jr (1990). *The Pharmaceutical Basis of Therapeutics*, 8th ed., edited by A. G. Gilman, T. W. Rall, S. Nies & P. Taylor, ch. 43, pp. 1008–1017. Oxford: Pergamon Press.